



Contents lists available at ScienceDirect

Nuclear Instruments and Methods in Physics Research B

journal homepage: www.elsevier.com/locate/nimb

Rate capability of a cryogenic stopping cell for uranium projectile fragments produced at 1000 MeV/u

M.P. Reiter^a, A.-K. Rink^{a,1}, T. Dickel^{a,b}, E. Haettner^{a,b}, F. Heiße^{a,b,c}, W.R. Plaß^{a,b,*}, S. Purushothaman^b, F. Amjad^b, S. Ayet San Andrés^{a,b}, J. Bergmann^a, D. Blum^b, P. Dendooven^d, M. Diwisch^a, J. Ebert^a, H. Geissel^{a,b}, F. Greiner^a, C. Hornung^a, C. Jesch^a, N. Kalantar-Nayestanaki^d, R. Knöbel^{a,b}, J. Lang^a, W. Lippert^a, I. Miskun^{a,b}, I.D. Moore^e, C. Nociforo^b, M. Petrick^a, S. Pietri^b, M. Pfützner^{b,f}, I. Pohjalainen^e, A. Prochazka^b, C. Scheidenberger^{a,b}, M. Takechi^b, Y.K. Tanaka^b, H. Weick^b, J.S. Winfield^b, X. Xu^{a,b}

^a II. Physikalisches Institut, Justus-Liebig-Universität Gießen, 35392 Gießen, Germany

^b GSI Helmholtzzentrum für Schwerionenforschung GmbH, 64291 Darmstadt, Germany

^c Institut für Kern- und Teilchenphysik, Technische Universität Dresden, 01069 Dresden, Germany

^d KVI-Center for Advanced Radiation Technology, University of Groningen, 9747 AA Groningen, The Netherlands

^e University of Jyväskylä, FI-40014 Jyväskylä, Finland

^f Faculty of Physics, University of Warsaw, 00-681 Warszawa, Poland

ARTICLE INFO

Article history:

Received 1 September 2015

Received in revised form 2 December 2015

Accepted 10 December 2015

Available online xxxxx

Keywords:

Cryogenic gas-filled stopping cell

Rate capability

Space charge

Extraction efficiency

Extraction time

ABSTRACT

At the Low-Energy Branch (LEB) of the Super-FRS at FAIR, projectile and fission fragments will be produced at relativistic energies, separated in-flight, energy-bunched, slowed down and thermalized in a cryogenic stopping cell (CSC) filled with ultra-pure He gas. The fragments are extracted from the stopping cell using a combination of DC and RF electric fields and gas flow. A prototype CSC for the LEB has been developed and successfully commissioned at the FRS Ion Catcher at GSI. Ionization of He buffer gas atoms during the stopping of energetic ions creates a region of high space charge in the stopping cell. The space charge decreases the extraction efficiency of stopping cells since the high amount of charge distorts the applied DC electric drag fields. Thus the understanding of space charge effects is of great importance to make full use of the high yields at future RIB facilities such as the Super-FRS at FAIR. For this purpose a detailed study of space charge effects in the CSC was performed using experiments and simulations. The dependence of the extraction efficiency, the extraction time and the temporal ion extraction profile on the intensity of the impinging beam and the electric field strength was studied for two different ²³⁸U projectile fragments produced at 1000 MeV/u and separated with the FRS. Good agreement between experiments and simulations was found.

© 2015 Elsevier B.V. All rights reserved.

1. Introduction

The slowing down and thermalization of exotic nuclei produced in-flight is a powerful and universal method to provide cooled nuclei almost at rest for low-energy precision experiments, e.g. with traps or lasers [1]. Thermalization takes place in a stopping cell filled with a noble gas, typically He. Most nuclei survive the thermalization process as singly or doubly charged ions and can be extracted from the cell using a combination of electric DC and

RF fields and the gas flow through an extraction nozzle. The ions can be captured into an RF ion guide and transferred to experiments. The origin of this method is based on the IGISOL technique developed in Jyväskylä [2]. It was pioneered in RIKEN [3] and at Argonne National Laboratory [4]. In recent years several further low-energy RIB facilities have been constructed based on the combination of the in-flight method with a gas-filled stopping cell, both for fusion products and projectile fragments [5–7].

One of the challenges of this approach is the operation of stopping cells with high beam intensities [8–12]. Ions that are thermalized in the stopping cell or pass through cause ionization of the buffer gas and create high densities of He ion–electron pairs. The motion of the electrons is fast compared to that of the thermalized ions. Thus they are quickly removed from the gas by the extraction

* Corresponding author at: II. Physikalisches Institut, Justus-Liebig-Universität Gießen, 35392 Gießen, Germany.

E-mail address: Wolfgang.R.Plass@exp2.physik.uni-giessen.de (W.R. Plaß).

¹ Part of doctoral thesis, Justus-Liebig-Universität Gießen, in preparation.

fields. The He ions however move with similar velocities as the thermalized ions and cause a blow-up of the ion population, which leads to losses on the electrodes of the stopping cell. The onset of this effect may occur already at rates of a few hundred stopped ions per second, since, depending on the stopping gas density and the energy and nuclear charge of the ion, a single stopped ion produces up to 10^7 He ion–electron pairs during the thermalization in the He stopping gas in current stopping cells. At higher beam intensities plasma effects occur. In this environment, the plasma compensates the external electric fields, such that the ions are trapped and lost due to recombination processes. This loss in efficiency is particularly harmful if the ions of interest are produced with orders of magnitude lower rate as compared to the unwanted species. High-intensity operation is particularly challenging in the case of ions produced at relativistic energies. Here, the energy straggling after slowing-down is much larger than that in the case of ions that have been produced at lower kinetic energies. Areal densities of up to several 10 mg/cm^2 may be required for efficient stopping even after energy-bunching [13]. Thus stopping cells with high gas-densities are required, which consequently need to deal with high ionization densities.

At the Low-Energy Branch (LEB) [13,14] of the Super-FRS [15] at the Facility for Antiproton and Ion Research (FAIR), projectile and fission fragments will be slowed down and thermalized in a stopping cell. They will then be extracted and transferred to the experiments MATS and LaSpec [16] for high-accuracy mass measurements, for in-trap and trap-assisted decay spectroscopy as well as for laser spectroscopy experiments, respectively. Recently, a prototype of the cryogenic stopping cell (CSC) for the LEB has been developed [7,17] and commissioned as part of the FRS Ion Catcher experiment at GSI [18] with uranium projectile fragments produced at 1000 MeV/u , i.e. with ions at much higher kinetic energies than any other stopping cell for exotic nuclei worldwide [19]. As part of the commissioning, the rate capability of the CSC and the space charge effects occurring in it have been studied. Further insight has been gained from simulation studies. The results are presented here.

2. Experiment

The experiments have been performed at the FRS [20] at GSI. The experimental setup has been described in detail elsewhere [18,19,17]. In two separate experiments, ^{221}Ac ions (half-life $T_{1/2} = 52 \text{ ms}$) and ^{213}Fr ions ($T_{1/2} = 34.6 \text{ s}$) were produced via projectile fragmentation of a ^{238}U primary beam at an energy of 1000 MeV/u in a beryllium target with an areal density of 1.629 g/cm^2 . The target was followed by a 0.223 g/cm^2 Nb stripper to reach the highest charge state at this energy. The ^{221}Ac and ^{213}Fr ions were separated in flight from the primary beam and other reaction products and were energy-bunched using twofold magnetic rigidity analysis and a 4.063 g/cm^2 Al monoenergetic degrader located at the central focal plane of the FRS. The identification of the ions was performed using the particle detectors of the FRS. After further slowing-down in a homogeneous degrader at the final focal plane, the ions were injected into the CSC. The stopping volume of the CSC has a length of 105.4 cm and a diameter of 25 cm .

The ^{221}Ac ions were thermalized in the He gas at a pressure of 49 mbar and a temperature of 74 K , corresponding to an areal density of 3.3 mg/cm^2 . They were extracted from the CSC into an RFQ quadrupole beam line [18] and collected on a thin foil in front of a Si detector. Using the Si detector they were identified and counted by their characteristic alpha decay energies.

The ^{213}Fr ions were thermalized in the He gas at a pressure of 63 mbar and a temperature of 86 K , corresponding to an areal den-

sity of 3.7 mg/cm^2 . After extraction from the CSC, they were transferred through the RFQ quadrupole beam line to a multiple-reflection time-of-flight mass spectrometer (MR-TOF-MS) [21]. They were identified by their time-of-flight after 128 turns in the MR-TOF-MS at a mass resolving power of about 200,000. For the rate measurements the broadband mode of the MR-TOF-MS without reflections in the analyzer was used. Compared to the decay measurement using the Si detector, the MR-TOF-MS has the advantage that the method is universally applicable regardless of the decay properties of the particles, e.g. even in the case of long half-lives.

In both experiments, the optimum range of the ions for most efficient stopping in the CSC was tuned by varying the homogeneous degrader in front of the CSC and maximizing the ratio of extracted to injected ^{221}Ac or ^{213}Fr ions. The overall efficiency of the thermalization process, given by the product of stopping efficiency and extraction efficiency, was measured for different beam intensities. The stopping efficiencies were determined from a measurement of the range distribution and the known areal density of the stopping cell. The extraction efficiencies could then be calculated as the ratio of overall efficiency to stopping efficiency. The beam intensities were measured using a scintillator mounted in front of the stopping cell. Ionization of the He gas in the CSC resulted in an electric current on a stainless steel window located at the entrance of the DC cage inside the CSC. In the experiment with ^{213}Fr this current was measured and allowed the determination of the number of electrons produced per ion injected into the CSC. Each rate capability study was performed for two different DC field strengths applied along the length of the CSC. The measurements were performed using either long primary beam spills ($\sim 4 \text{ s}$) or short spills ($4\text{--}6 \text{ ms}$). At the same overall number of ions, short spills give rise to stronger space charge effects in the CSC than long spills, since the rate (ions/s) is larger. The conversion of the rate with short or long spills to the equivalent rate of a DC beam is intricate however, since it depends on the extraction time from the CSC and hence also on the intensity (see discussion below).

3. Simulations

To complement the measurements, simulations of space charge effects occurring in the CSC were performed [22]. The longitudinal and transverse distributions of the stopped ions and of the ionization created in the CSC were obtained using the simulation programs MOCADI [23] and SRIM [24]. These distributions were used as starting distributions for trajectory calculations of the ions in the CSC, which take into account the externally applied electric field, the space charge field created by the ions and the mobility and diffusion of the ions in the He stopping gas. The trajectory simulations were performed using the simulation package SIMION 8.1.1.32 [25]. The external electric fields were calculated from the voltages applied to the DC electrodes of the CSC and the known geometry of the electrodes. The space charge fields were obtained using the Poisson solver of SIMION, which implements a particle-in-cell method. While the external electric potential is calculated only once, the space charge potential needs to be re-calculated at every time step of the simulation. The influence of the He stopping gas was taken into account using the ion mobility μ . The equation of motion of an ion with mass m and charge e in the electric field \mathbf{E} is then given by

$$\ddot{\mathbf{r}} = \frac{e}{m} \left(\mathbf{E} - \frac{\dot{\mathbf{r}}}{\mu} \right) \quad (1)$$

where $\ddot{\mathbf{r}}$ and $\dot{\mathbf{r}}$ denote the ion acceleration and velocity, respectively. The effect of diffusion was modeled by applying an offset in the

position in each Cartesian direction of each ion per simulation time step Δt . The offset was drawn randomly from a Gaussian distribution with a standard deviation of

$$\sigma = \sqrt{2D\Delta t} \quad (2)$$

where D is the diffusion coefficient. The diffusion coefficient was obtained from the ion mobility using the Einstein relation

$$D = \frac{\mu k_B T}{e} \quad (3)$$

where k_B is Boltzmann's constant and T the temperature. At cryogenic temperature, the mobilities of heavier singly or doubly charged atomic cations in He gas are very similar; a reduced ion mobility of $17.5 \text{ cm}^2/(\text{Vs})$ is assumed for $^{221}\text{Ac}^+$ and for $^{213}\text{Fr}^+$ [26,27]. Under the conditions of the experiment, the He ions occur primarily as trimers He_3^+ ; their reduced mobility amounts to about $18 \text{ cm}^2/(\text{Vs})$ [28,26]. In some of the experiments, more than 10^{11} He ions were present in the CSC at the same time. In order to have a reasonable computation time for each simulation of typically 12–24 h regardless of the beam intensity to be simulated, only 10^4 ions were simulated and a charge weighting factor, which increases the charge repulsion in the simulation, between 10^3 and 10^8 was applied to obtain He ion rates between 10^7 and 10^{12} per spill.

The ion motion at the RF carpet or in the nozzle was not included in the simulation. Rather, an ion was considered to be successfully extracted from the CSC when it reached the RF carpet. However, for extraction time simulations the transport time for the ion motion along the carpet was added to that obtained for the motion to the carpet. Here it was assumed that the transport along the carpet occurs with a velocity according to the ion mobility of the ions without RF fields. The validity of the simulations was tested against several analytical models and good agreement was found.

Comparison of the measurements and the simulations requires knowledge about the number of He ion–electron pairs created per ion impinging on the CSC. The corresponding conversion factor depends on the energy the ion deposits in the CSC and hence on the beam energy, the beam composition, the range of the beam components and the areal density of the stopping cell. Taking into account that the mean energy loss per He ion–electron pair amounts to 41 eV [29], 6.4×10^6 He ion–electron pairs were created per impinging ion in the experiment with ^{221}Ac and 9.5×10^6 He ion–electron pairs in the experiment with ^{213}Fr . The latter value is compatible with the measurement of the electron current on the entrance window of the DC cage of the CSC (see above).

4. Results and discussion

In Fig. 1 the simulated trajectories of the ions injected into the CSC as well as the trajectories of the He ions created in the CSC are shown for two different beam intensities. The ions enter the CSC from the left-hand side, and the electric DC field pulls them towards the extraction side of the CSC on the right-hand side. At an ionization rate of $10^{11} \text{ He}_3^+/\text{s}$ all ions are transported to the RF carpet. However, at a rate of $10^{12} \text{ He}_3^+/\text{s}$ the space charge of the ions causes a deflection of the ions. Ions starting in the entrance region of the CSC are deflected towards the ring electrodes of the CSC and are lost. The equipotential lines shown in Fig. 1 illustrate the defocusing effect of the overall electric field. Only ions originating from locations closer to the exit side of the CSC are extracted successfully. This effect has also been observed for other stopping cells, see e.g. [9]. In general the strength of the deflection increases with ionization density, and the region of ions to be successfully

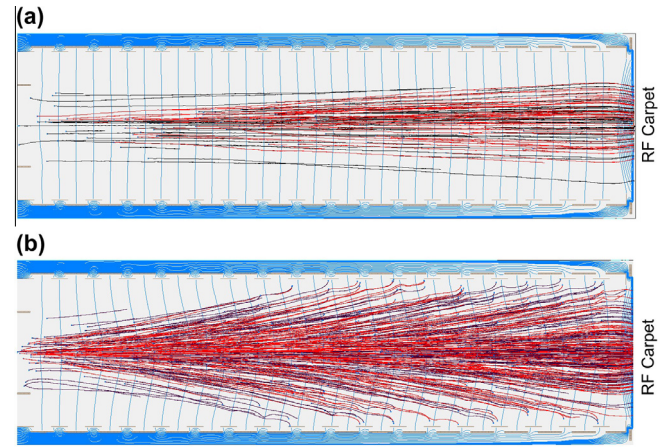


Fig. 1. Equipotential lines (blue) of the electric field and trajectories of stopped ions (black) and He ions (red) in the CSC at two different ionization rates. The ions enter the CSC from the left and are transported to the RF carpet on the exit side of the CSC using electric DC fields. (a) At an ionization rate of $10^{11} \text{ He}_3^+/\text{s}$ all ions are transported to the RF carpet. (b) At an ionization rate of $10^{12} \text{ He}_3^+/\text{s}$ the ions stopped in the entrance region of the CSC are defocused by the space charge and impinge on the electrodes of the CSC. (For interpretation of the references to colour in this figure legend, the reader is referred to the web version of this article.)

extracted is reduced to smaller volumes close to the extraction nozzle of the CSC. Because of this (i) the extraction efficiency decreases and (ii) the mean extraction time of the successfully extracted ions decreases. In the following, these two consequences will be investigated quantitatively.

In order to convert the results of measurements and simulations with pulsed bunches of ions to the equivalent results obtained with a DC beam, a conversion factor was derived from simulations. The simulations show that for spill lengths much shorter than the time required for removal of the charges from the CSC (i.e. for spill lengths of a few milliseconds or less) the space charge effects are the same for a given number of ions regardless of the ion rate. Conversely, for spill lengths much longer than the time required for removal of charges the strength of the space charge effects only depends on the ion rate regardless of the number of ions per spill. The transition between the two regimes is defined by a characteristic time t_{char} . Simulations reveal that a good approximation of the characteristic time is given by the time it takes until 90% of the He ions created have impinged on the electrodes [22]. It is on the order of the extraction time. The condition under which the space charge effects for a DC beam and for a pulsed beam are equivalent are then given in approximation by

$$I = \frac{N}{\sqrt{t_{\text{spill}}^2 + t_{\text{char}}^2}} \quad (4)$$

where I is the ionization rate of the DC beam in ion–electron pairs per unit time, N is the number of ion–electron pairs created by the pulsed beam and t_{spill} is the spill length of the pulsed beam. The spill length and the characteristic time are added quadratically in Eq. (4) because the respective limitations can be considered to be independent of each other. The characteristic time strongly depends on the beam intensity. Under the conditions of the experiment and for a spill length of 1 ms it amounts to about 50 ms at low beam intensities; for 10^{13} He ion–electron pairs it decreases to less than one millisecond. Despite the conversion to the equivalent of a DC beam, the simulations shown here were performed with the same spill lengths as used in the corresponding experiments.

The extraction efficiencies for ^{221}Ac and ^{213}Fr measured as a function of the beam rate are shown in Fig. 2. Spills with a length

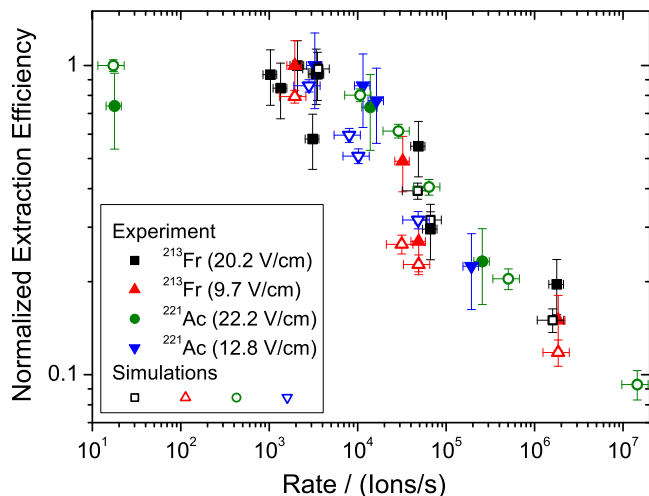


Fig. 2. Extraction efficiencies for ²²¹Ac and ²¹³Fr in dependence of the beam rate from experiments (solid symbols) and simulations (open symbols) for two different electric DC field strengths each. Every data series has been normalized independently to a maximum extraction efficiency of unity.

of 4–6 ms were used; the time between spills was about 8 s and 4 s, respectively. The rate was converted to the equivalent rate of a DC beam and the extraction efficiencies were normalized to the maximum of each measurement series. Up to a rate of about 10⁴ ions/s injected into the CSC, the extraction efficiency is constant. For higher beam rates, the extraction efficiency decreases strongly with increasing rate and drops to about 10% of its original value at 10⁷ ions/s. A higher DC field strength increases the extraction efficiency at a given beam rate, or conversely, it increases the rate for a given extraction efficiency, however the gain in rate for an increase in field strength by a factor of two is only about 40% in the simulations. The results of the simulations are in good agreement with the measured results. This is a clear indication that the reduction of the efficiency with increasing beam rate is due to space charge effects along the DC cage of the CSC, rather than plasma effects or space charge effects at the RF carpet or in the nozzle region of the CSC. The charge density of the ions transported by the RF carpet can be assumed to be significantly higher in the central region of the RF carpet. However, the simulations show that due to their light mass, the motion of the helium ions in the RF field of the RF carpet is unstable, i.e. the helium ions are not repelled by the RF field but impinge on the conducting sections of the RF carpet. The majority of the space charge is due to the helium ions rather than the much heavier projectile fragments, which are transported by the RF carpet. The overall space charge at the RF carpet can therefore be assumed not to be higher than throughout the stopping volume.

Mass spectra of ions extracted from the CSC at different beam rates were acquired with the MR-TOF-MS. They are dominated by the ions of interest, which have been stopped in the CSC [19]. Furthermore, within the uncertainties of the measurement, the ratio of the number of contaminant ions, such as ions with adducts or molecular contaminants, to the number of ions of interest does not depend significantly on the beam rate.

Long-term operation of the CSC at rates of about 10⁶ ions/s injected into the CSC did not result in noticeable changes to the RF carpet, e.g. arising from charging of the insulating sections of the carpet. Short-term operation with up to 8×10^8 ions injected into the cell ignited a steady discharge, but did not cause damage to the CSC.

A measurement of the extraction time as a function of the beam rate was performed using short spills of ²²¹Ac by a method

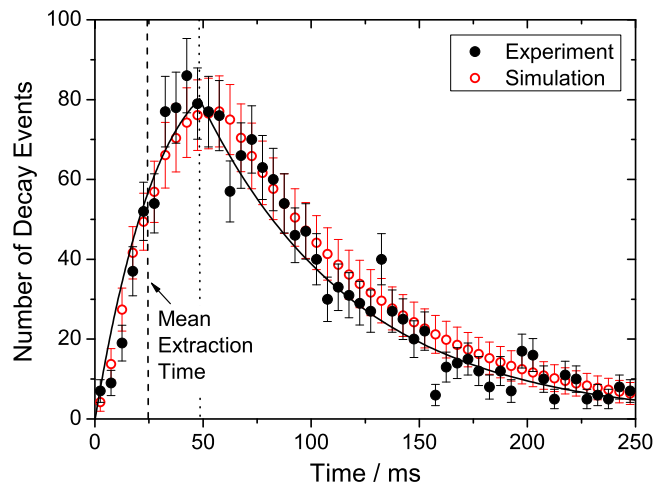


Fig. 3. Extraction time measurement of ²²¹Ac ions from the CSC. The solid symbols show the measured number of ²²¹Ac decay events recorded with the Si detector as a function of time after their injection as bunches with a temporal width of 4–6 ms into the CSC; the time between spills was about 8 s. The curve is a fit to the data [19]. 650 ions were injected into the CSC per spill. The open symbols show the results of corresponding simulations. The number of decays obtained in the simulation were scaled to match the experimental values.

described previously [19]. After injection of the ion bunch into the CSC, the decays of the extracted ²²¹Ac ions were measured on the Si detector located behind the CSC. Fig. 3 shows the time dependence of the decay rate for a beam rate of 650 ions per spill and a DC field strength of 22.2 V/cm. After injection of the ²²¹Ac ions activity accumulates on the Si detector and the decay rate increases. After 48 ms the last ²²¹Ac ions are extracted and the decay rate reaches a maximum. After that the ²²¹Ac nuclei remaining on the Si detector decay further. The mean extraction time is half that of the maximum extraction time, i.e. 24 ms. Good agreement with the corresponding simulation is achieved.

The extraction times determined by measurements and simulations as a function of the beam rate are shown in Fig. 4. Up to a rate

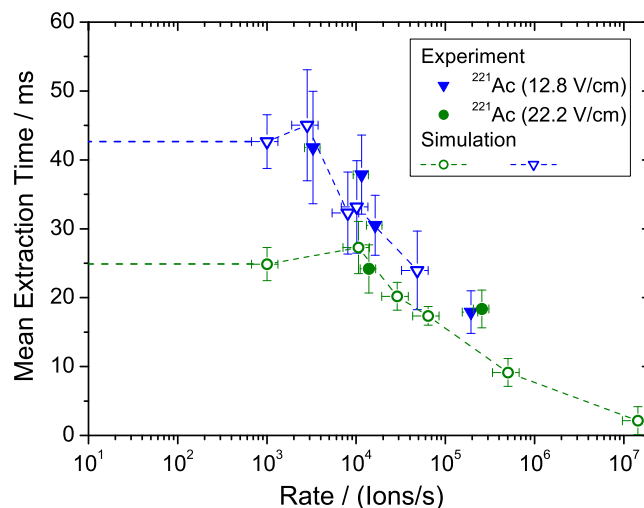


Fig. 4. Mean extraction time of ²²¹Ac ions from the CSC as a function of the beam rate for two different mean electric DC field strengths along the body of the CSC. The pressure and the temperature in the CSC amounted to 49 mbar and 74 K, respectively. The solid symbols show measured values using ion bunches injected into the CSC with a temporal width of 4–6 ms; the time between spills was about 8 s. The experimental results are compared with the results of simulations (open symbols).

of about 10^3 ions/s injected into the CSC the extraction times are roughly constant. For the higher DC field strength, shorter extraction times are achieved. The values obtained by simulations agree with the results predicted by the ion mobilities. For higher beam rates the extraction time decreases and the difference between the extraction times at high and low DC field strengths reduces. The measurements and the simulations are in fair agreement, although for the higher DC field strength only two experimental data points are available. The decrease can be explained by the fact that with increasing space charge effects only ions close to the nozzle region of the CSC are extracted. Since they have a shorter distance to travel to the nozzle than ions from other regions in the CSC, the extraction time is reduced. A higher DC field strength increases the region, from which ions are extracted. Thus for a higher DC field strength the average distance the ions need to travel is larger, but the ion velocity is also larger. These two effects compensate each other to a certain extent, reducing the difference in the extraction times at high and low field strengths.

5. Conclusions and outlook

The extraction efficiencies, extraction times and extraction profiles of a CSC have been studied in experiments and simulations using ^{238}U projectile fragments produced at 1000 MeV/u. Up to a rate of about 10^4 ions/s injected into the CSC the extraction efficiencies and extraction times are constant; at higher rates the extraction efficiencies and extraction times decrease. This behavior can be explained by space charge effects, which cause a deflection of the ions in the CSC towards the electrodes, such that with increasing beam rate only ions stopped closer to the extraction nozzle can be extracted. The measurements and simulations show good agreement.

The conditions chosen for the study are challenging (i) since the high energy of the ions leads to a large energy straggling after slowing-down and consequently requires a high stopping gas density and (ii) because of the high nuclear charge of the fragments. Since the energy deposition roughly scales with the square of the nuclear charge, the rate capability of the CSC for lighter elements will be much higher.

The study shows that the highest rate capability is achieved at large DC field strengths. Furthermore a good separation of the nuclide of interest from beam contaminants with a longer range is required to avoid additional ionization of the He stopping gas. Since with the present CSC the range distribution is significantly larger than the areal density of the CSC it may be advantageous to shift the mean range of the nuclides of interest such that the long-range component of the nuclides of interest is stopped.

Several approaches have been proposed to further increase the rate capability of stopping cells, including larger stopping volumes to reduce the charge density, the implementation of RF structures that surround the whole stopping volume [30] and the use of magnetic fields [31]. We have developed a novel concept of a CSC with orthogonal extraction [32]. Besides much higher areal density and shorter extraction times, this CSC will have a rate capability exceeding 10^7 ions/s. This concept will be realized for the stopping cell for the LEB of the Super-FRS at FAIR.

Acknowledgements

We thank K.-H. Behr, T. Blatz, A. Brünle, C. Karagiannis, A. Kratz, C. Lotze, C. Schlör, B. Szczepanczyk, F. Schreuder, J. Siebring, T. Wasem and R. Weiß for excellent technical support. Financial support was provided within the collaboration agreement between the GSI Helmholtzzentrum für Schwerionenforschung GmbH and KVI, University of Groningen, by the German Federal Ministry for Edu-

cation and Research (BMBF) under contract No. 05P12RGFN8, by the Hessian Ministry for Science and Art (HMWK) through the LOEWE Center HICforFAIR, by HGS-HiRe, by the Justus-Liebig-Universität Gießen and GSI under the JLU-GSI strategic Helmholtz partnership agreement, and by the European Community FP7 – Capacities, contract ENSAR No. 262010.

References

- [1] M. Wada, Genealogy of gas cells for low-energy RI-beam production, *Nucl. Instrum. Methods B* 317 (2013) 450–456.
- [2] J. Årje, K. Valli, Helium-jet ion guide for an on-line isotope separator, *Nucl. Instrum. Methods* 179 (1981) 535–539.
- [3] M. Wada, Y. Ishida, T. Nakamura, Y. Yamazaki, T. Kambara, H. Ohya, Y. Kanai, T.M. Kojima, Y. Nakai, N. Ohshima, A. Yoshida, T. Kubo, Y. Matsuo, Y. Fukuyama, K. Okada, T. Sonoda, S. Ohtani, K. Noda, H. Kawakami, I. Katayama, Slow RI-beams from projectile fragment separators, *Nucl. Instrum. Methods B* 204 (2003) 570–581.
- [4] G. Savard, J. Clark, C. Boudreau, F. Buchinger, J. Crawford, H. Geissel, J. Greene, S. Gulick, A. Heinz, J.K.P. Lee, A. Levand, M. Maier, G. Münzenberg, C. Scheidenberger, D. Seweryniak, K.S. Sharma, G. Sprouse, J. Vaz, J.C. Wang, B.J. Zabransky, Z. Zhou, Development and operation of gas catchers to thermalize fusion-evaporation and fragmentation products, *Nucl. Instrum. Methods B* 204 (2003) 582–586.
- [5] L. Weissman, D.J. Morrissey, G. Bollen, D.A. Davies, E. Kwan, P.A. Lofy, P. Schury, S. Schwarz, C. Sumithrarachchi, T. Sun, R. Ringle, Conversion of 92 MeV/u ^{38}Ca / ^{37}K projectile fragments into thermalized ion beams, *Nucl. Instrum. Methods A* 540 (2005) 245–258.
- [6] J. Neumayr, L. Beck, D. Habs, S. Heinz, J. Szerypo, P. Thierolf, V. Varentsov, F. Voit, D. Ackermann, D. Beck, M. Block, Z. Di, S. Eliseev, H. Geissel, F. Herfurth, F. Heberger, S. Hofmann, H.-J. Kluge, M. Mukherjee, G. Münzenberg, M. Petrick, W. Quint, S. Rahaman, C. Rauth, D. Rodriguez, C. Scheidenberger, G. Sikler, Z. Wang, C. Weber, W. Plaß, M. Breitenfeldt, A. Chaudhuri, G. Marx, L. Schweikhard, A. Dodonov, Y. Novikov, M. Suhonen, The ion-catcher device for SHIPTRAP, *Nucl. Instrum. Methods B* 244 (2006) 489–500.
- [7] M. Ranjan, S. Purushothaman, T. Dickel, H. Geissel, W.R. Plaß, D. Schäfer, C. Scheidenberger, J. Van de Walle, H. Weick, P. Dendooven, New stopping cell capabilities: RF carpet performance at high gas density and cryogenic operation, *Eur. Phys. Lett.* 96 (2011) 52001.
- [8] M. Huyse, M. Facina, Y. Kudryavtsev, P.V. Duppen, Intensity limitations of a gas cell for stopping, storing and guiding of radioactive ions, *Nucl. Instrum. Methods B* 187 (2002) 535–547.
- [9] A. Takamine, M. Wada, Y. Ishida, T. Nakamura, K. Okada, Y. Yamazaki, T. Kambara, Y. Kanai, T.M. Kojima, Y. Nakai, N. Ohshima, A. Yoshida, T. Kubo, S. Ohtani, K. Noda, I. Katayama, P. Hostain, V. Varentsov, H. Wollnik, Space-charge effects in the catcher gas cell of a rf ion guide, *Rev. Sci. Instrum.* 76 (2005) 103503.
- [10] D.J. Morrissey, Extraction of thermalized projectile fragments from gas, *Eur. Phys. J. Special Top.* 150 (2007) 365–366.
- [11] I.D. Moore, New concepts for the ion guide technique, *Nucl. Instrum. Methods B* 266 (2008) 4434–4441.
- [12] M. Facina, C. Bachelet, M. Block, G. Bollen, D. Davies, C.M. Folden III, C. Guenaut, J. Huikari, E. Kwan, D.J. Morrissey, G.K. Pang, A. Prinke, R. Ringle, J. Savory, P. Schury, S. Schwarz, C. Sumithrarachchi, T. Sun, Charged particle transport and extraction studies in the NSCL gas cell for stopping radioactive fragments, *Nucl. Instrum. Methods B* 266 (2008) 4471–4474.
- [13] J.S. Winfield, H. Geissel, J. Gerl, G. Münzenberg, C. Nociforo, W.R. Plaß, C. Scheidenberger, H. Weick, M. Winkler, M.I. Yavor, A versatile high-resolution magnetic spectrometer for energy compression, reaction studies and nuclear spectroscopy, *Nucl. Instrum. Methods A* 704 (2013) 76–83.
- [14] H. Geissel, J.S. Winfield, G.P.A. Berg, B. Franczak, N. Iwasa, G. Münzenberg, C. Nociforo, W.R. Plaß, C. Scheidenberger, H. Weick, M. Winkler, M. Yavor, Dispersion-matched spectrometer in the low-energy branch of the Super-FRS for high-resolution measurements with large-emittance relativistic fragment beams, *Nucl. Instrum. Methods B* 317 (2013) 277–283.
- [15] H. Geissel, H. Weick, M. Winkler, G. Münzenberg, V. Chichikine, M. Yavor, T. Aumann, K.H. Behr, M. Böhmer, A. Brünle, K. Burkard, J. Benlliure, D. Cortina-Gil, L. Chulkov, A. Dael, J.-E. Ducret, H. Emling, B. Franczak, J. Friese, B. Gastineau, J. Gerl, R. Gernhäuser, M. Hellström, B. Jonson, J. Kojouharova, R. Kulesa, B. Kindler, N. Kurz, B. Lommel, W. Mittig, G. Moritz, C. Mühle, J.A. Nolen, G. Nyman, P. Roussel-Chomaz, C. Scheidenberger, K.-H. Schmidt, G. Schrieder, B. Sherrill, H. Simon, K. Sümmerer, N.A. Tahir, V. Vysotsky, H. Wollnik, A.F. Zeller, The Super-FRS project at GSI, *Nucl. Instrum. Methods B* 204 (2003) 71–85.
- [16] D. Rodriguez et al., MATS and LaSpec: high-precision experiments using ion traps and lasers at FAIR, *Eur. Phys. J. Special Top.* 183 (2010) 1–123.
- [17] M. Ranjan, P. Dendooven, S. Purushothama, T. Dickel, M.P. Reiter, S. Ayet, E. Haettner, I.D. Moore, N. Kalantar-Nayestanaki, H. Geissel, W.R. Plaß, D. Schäfer, C. Scheidenberger, F. Schreuder, H. Timersma, J. Van de Walle, H. Weick, Design, construction and cooling system performance of a prototype cryogenic stopping cell for the Super-FRS at FAIR, *Nucl. Instrum. Methods A* 770 (2015) 87–97.

- [18] W.R. Plaß, T. Dickel, S. Purushothaman, P. Dendooven, H. Geissel, J. Ebert, E. Haettner, C. Jesch, M. Ranjan, M.P. Reiter, H. Weick, F. Amjad, S. Ayet, M. Diwisch, A. Estrade, F. Farinon, F. Greiner, N. Kalantar-Nayestanaki, R. Knöbel, J. Kurcewicz, J. Lang, I. Moore, I. Mukha, C. Nociforo, M. Petrick, M. Pfuetzner, S. Pietri, A. Prochazka, A.-K. Rink, S. Rinta-Antila, D. Schäfer, C. Scheidenberger, M. Takechi, Y.K. Tanaka, J.S. Winfield, M.I. Yavor, The FRS Ion Catcher – a facility for high-precision experiments with stopped projectile and fission fragments, *Nucl. Instrum. Methods B* 317 (2013) 457–462.
- [19] S. Purushothaman, M.P. Reiter, E. Haettner, P. Dendooven, T. Dickel, H. Geissel, J. Ebert, C. Jesch, W.R. Plaß, M. Ranjan, H. Weick, F. Amjad, S. Ayet, M. Diwisch, A. Estrade, F. Farinon, F. Greiner, N. Kalantar-Nayestanaki, R. Knöbel, J. Kurcewicz, J. Lang, I. Moore, I. Mukha, C. Nociforo, M. Petrick, M. Pfuetzner, S. Pietri, A. Prochazka, A.-K. Rink, S. Rinta-Antila, C. Scheidenberger, M. Takechi, Y.K. Tanaka, J.S. Winfield, M.I. Yavor, First online results of a cryogenic stopping cell with short-lived heavy uranium fragments produced at 1000 MeV/u, *Eur. Phys. Lett.* 104 (2013) 42001.
- [20] H. Geissel, P. Armbruster, K.H. Behr, A. Brünle, K. Burkard, M. Chen, H. Folger, B. Franczak, H. Keller, O. Klepper, B. Langenbeck, F. Nickel, E. Pfeng, M. Pfützner, E. Roeckl, K. Rykaczewski, I. Schall, D. Schardt, C. Scheidenberger, K.H. Schmidt, A. Schröter, T. Schwab, K. Sümmerer, M. Weber, G. Münzenberg, T. Brohm, H.G. Clerc, M. Fauerbach, J.J. Gaimard, A. Grewe, E. Hanelt, B. Knödler, M. Steiner, B. Voss, J. Weckenmann, C. Ziegler, A. Magel, H. Wollnik, J.P. Dufour, Y. Fujita, D.J. Vieira, B. Sherrill, The GSI projectile fragment separator (FRS): a versatile magnetic system for relativistic heavy ions, *Nucl. Instrum. Methods B* 70 (1992) 286–297.
- [21] T. Dickel, W.R. Plaß, A. Becker, U. Czok, H. Geissel, E. Haettner, C. Jesch, W. Kinsel, M. Petrick, C. Scheidenberger, M.I. Yavor, A high-performance multiple-reflection time-of-flight mass spectrometer and isobar separator for the research with exotic nuclei, *Nucl. Instrum. Methods A* 777 (2015) 172–188.
- [22] F. Heiße, Investigation of the cryogenic gas-filled stopping cell for the FRS Ion Catcher (MSc thesis), Technische Universität Dresden, 2015.
- [23] N. Iwasa, H. Geissel, G. Münzenberg, C. Scheidenberger, T. Schwab, H. Wollnik, MOCADI, a universal Monte Carlo code for the transport of heavy ions through matter within ion-optical systems, *Nucl. Instrum. Methods B* 126 (1997) 284–289.
- [24] J.F. Ziegler, M.D. Ziegler, J.P. Biersack, SRIM the stopping and range of ions in matter, *Nucl. Instrum. Methods B* 268 (2010) 1818–1823.
- [25] D.J. Manura, D.A. Dahl, SIMION 8.0 User Manual, Sci. Instrument Services Inc, Idaho Nat. Lab., 2006.
- [26] S. Purushothaman, Superfluid Helium and Cryogenic Noble Gases as Stopping Media for Ion Catchers (Ph.D. thesis), University of Groningen, 2008.
- [27] L.A. Viehland, Zero-field mobilities in helium: highly accurate values for use in ion mobility spectrometry, *Int. J. Ion Mobility Spectrom.* 15 (2012) 21–29.
- [28] P.L. Patterson, Temperature dependence of helium-ion mobilities, *Phys. Rev. A* 2 (1970) 1154.
- [29] W.R. Leo, *Techniques for Nuclear and Particle Physics Experiments*, Springer, Berlin, Heidelberg, New York, 1994.
- [30] G. Savard, S. Baker, C. Davids, A.F. Levand, E.F. Moore, R.C. Pardo, R. Vondrasek, B.J. Zabransky, G. Zinkann, Radioactive beams from gas catchers: the CARIBU facility, *Nucl. Instrum. Methods B* 266 (2008) 4086–4091.
- [31] G. Bollen, D.J. Morrissey, S. Schwarz, A study of gas stopping of intense energetic rare isotope beams, *Nucl. Instrum. Methods A* 550 (2005) 27–38.
- [32] T. Dickel, W.R. Plaß, H. Geissel, F. Heiße, I. Miskun, S. Purushothaman, M.P. Reiter, A.-K. Rink, C. Scheidenberger, Conceptual design of a novel next-generation cryogenic stopping cell for the Low-Energy Branch of the Super-FRS (this issue).